



**Technical  
Paper  
1973**

March 1982

NASA-TP-1973 19820012692

# Elastic-Plastic Finite-Element Analyses of Thermally Cycled Double-Edge Wedge Specimens

Albert Kaufman  
and Larry E. Hunt

LIBRARY COPY

LANGLEY RESEARCH CENTER  
LIBRARY, AREA  
HANFORD, VIRGINIA

**NASA**



# Elastic-Plastic Finite-Element Analyses of Thermally Cycled Double-Edge Wedge Specimens

Albert Kaufman  
and Larry E. Hunt  
*Lewis Research Center  
Cleveland, Ohio*



National Aeronautics  
and Space Administration

Scientific and Technical  
Information Branch



## Summary

Three-dimensional elastic and elastic-plastic stress-strain analyses using the MARC nonlinear, finite-element program were performed for double-edge wedge specimens subjected to thermal cycling in fluidized beds. Four cases involving different nickel-base turbine blade alloys tested under the same cycling conditions were analyzed in order to obtain the stress-strain histories at the locations of maximum total strain range for the purpose of developing life prediction methods. The alloys considered in this study were IN 100, Mar-M 200, NASA TAZ-8A, and René 80. Specimens of each alloy were thermally cycled by alternate 3-minute immersions in fluidized beds at 316° and 1088° C.

Elastic analysis results from the MARC program were in good agreement with previous results of elastic analyses from the NASTRAN and ISO3DQ finite-element programs. In the elastic-plastic analyses all four alloy cases exhibited plastic strain reversal during cycling. Comparison of MARC elastic and elastic-plastic analysis solutions showed that the maximum equivalent total strain ranges computed from the two types of analyses agreed within 3 percent but that the mean effective stresses were significantly different. Elastic analyses always resulted in compressive mean stresses. For two of the four alloys (IN 100 and NASA TAZ-8A) elastic-plastic analyses showed tensile mean stresses. In the highest plastic strain case (René 80) the mean stress increased in the compressive direction.

## Introduction

Hot-section components of aircraft gas turbine engines, such as combustor liners and turbine blades and vanes, are subject to cyclic thermomechanical loading, which can result in progressive fatigue damage and eventual cracking. Life prediction methods to assess the durability of these components have been under development at the NASA Lewis Research Center and are discussed in references 1 to 6. In order to apply these methods, it is first necessary to determine the stress-strain-temperature history of the part at the critical location where cracks will initiate.

As part of the life prediction studies at Lewis, wedge specimens have been thermally cycled in fluidized beds as described in reference 7. In these tests two fluidized beds were used to rapidly heat and cool prismatic bar specimens of double-edge wedge cross section. The bars were tested so that they failed by thermal fatigue cracking. Elastic stress-strain histories at the critical edge

locations of these specimens were obtained by performing three-dimensional finite-element structural analyses under a joint NASA-Air Force program. Lewis used the NASTRAN computer program (ref. 8); the Air Force Aero Propulsion Laboratory used the ISO3DQ computer program (ref. 9). The results of these elastic analyses are reported in reference 10. The experimental results from the fluidized-bed tests are summarized in references 11 and 12.

Nonlinear finite-element computer programs such as MARC (ref. 13) are available for more rigorous three-dimensional cyclic analyses of components involving inelastic plastic and creep strains. These programs have had some limited use as research analytical tools, as in the turbine blade airfoil studies described in references 14 to 16. However, nonlinear programs have not been applied to the design of engine hot-section parts mainly because of the extensive demands they make on computer resources and because of inadequacies in cyclic property data on superalloy materials and in the current state of transient heat transfer analysis methods. The NASA Lewis Research Center has instituted a program to improve the quality of the material and temperature input and to increase the computational efficiency of nonlinear structural analyses.

This study was conducted to determine the elastic-plastic stress-strain histories at the critical locations for double-edge wedge specimens that were thermally cycled in fluidized beds. These analytical results are required in order to use the experimental failure data in the development and evaluation of life prediction methods at Lewis.

The structural analyses were performed with the MARC nonlinear finite-element program using a combined isotropic-kinematic hardening model. The specimen geometry was modeled with 20-node, isoparametric, three-dimensional elements. A total of four cases involving different nickel-base turbine blade alloys (IN 100, Mar-M 200, NASA TAZ-8A, and René 80) were studied. The specimens analyzed were cycled in fluidized beds that were maintained at 316° and 1088° C with an immersion time of 3 minutes in each bed. For the same alloys, geometry, and thermal cycling conditions, elastic and elastic-plastic solutions from the MARC computer program were compared. In addition, to verify the analyses as much as possible, the MARC elastic solutions were compared with the elastic solutions from the NASTRAN and ISO3DQ computer programs given in reference 10. The ability of the analyses to predict critical locations for crack initiation could not be substantiated because of the uniformity of conditions over large regions of the wedge edges.

## Analytical Procedure

Elastic-plastic stress-strain states were calculated for double-edge wedge specimens of four alloys that were thermally cycled in fluidized beds. The alloys and test conditions for the four cases studied are presented in table I. Alloy compositions are given in reference 17.

### Input for Analyses

The specimen geometry, material properties, and thermal loading that were used as input to the structural analyses are described in this section.

**Geometry.**—The geometry of the double-edge wedge specimen is illustrated in figure 1. To be consistent with the NASTRAN and ISO3DQ analyses of reference 10, the leading-edge and trailing-edge radii were squared off to 1.02- and 1.53-millimeter lengths, respectively, for the finite-element model. Otherwise the finite-element model duplicated the geometry exactly.

**Material properties.**—The physical properties of the alloys were obtained from reference 10 and are reproduced in table II. An elastic-plastic analysis requires mechanical properties to define the work-hardening behavior under plastic straining; these data were obtained from reference 17 and are given in table III. Since the MARC program requires instantaneous coefficients of thermal expansion, the mean coefficient data in table II were converted to instantaneous values for input.

**Thermal loading.**—The transient temperature loading on the double-edge wedges was determined from thermocouple data. Calibration specimens of the four alloys were instrumented chordwise at the midspan with five embedded thermocouples and cycled in the fluidized beds (schematically shown in fig. 2). The location of the thermocouples at the wedge cross section is shown in figure 3. The Inconel 600 sheathed Chromel-Alumel thermocouples were mounted in grooves milled in the surface of the specimen and secured by a ceramic cement. The grooves were 0.56 millimeter wide and 0.5 millimeter deep. Other details of the installation and procedure are given in reference 7. The thermocouple outputs were cross-plotted to give midchord temperatures at the midspan at various time increments after immersion into the fluidized beds. These data are presented in figure 3 for the four cases analyzed. It was assumed that there was no temperature gradient through the thickness of the wedge.

Another set of thermocouple data was taken with five thermocouples mounted along the leading edge over half the span. These data revealed a longitudinal (along the span of the specimen) temperature gradient that varied with the different time increments. The maximum variation was about 16 percent greater at the ends of the wedge than at the midspan and occurred after 30 seconds of heating. However, for any one time increment the

ratio of the leading-edge midspan temperature to that of any other span location was nominally the same for all four alloys. A least-squares best-fit parabola was determined for each time increment and this is presented in table IV. This parabolic temperature variation along the span was assumed over the complete chord of the wedge.

The temperatures at the midspan were determined from the appropriate plot in figure 3. For locations other than midspan the temperatures were determined by using the midspan temperature modified by the values given in table IV. Therefore by using figure 3 and table IV the temperature distribution at any point of the wedge was determined.

### Methods of Analysis

Elastic and elastic-plastic stress-strain distributions in the wedge specimens were calculated from the MARC nonlinear, finite-element computer program. Computations were performed for 34 time increments (17 heating, 17 cooling) into which the thermal cycle was subdivided, as shown in figure 3. Elastic solutions using MARC were compared with the NASTRAN and ISO3DQ analyses of reference 10 in order to check the program input and the finite-element model. The elastic analyses were obtained by setting the material yield strength to a fictitiously high level. The elastic-plastic analyses only had to be performed for two cycles for IN 100, Mar-M 200, and NASA TAZ-8A in order to attain reasonably stable stress-strain hysteresis loops. The elastic-plastic analysis for the René 80 was performed for three cycles and was then terminated because of the excessive computing time involved, although the analysis had not yet shaken down to a stable stress-strain hysteresis loop.

Plasticity computations were based on incremental plasticity theory using the commonly used von Mises yield criterion and normality flow rule. The yield surface under reversed loading was found from the monotonic stress-strain behavior in conjunction with the combined isotropic-kinematic hardening model option described in reference 13. A preprocessor program converted the thermal loading data from the wedge specimen into the form of a sixth-order polynomial equation. A subroutine, which was inserted into MARC, interpolated from these equations for the local temperatures at the Gaussian integration points in the finite-element model. Another subroutine, which was inserted into the MARC program in the form of yield strengths and work-hardening slopes as functions of temperature, was used to determine the stress-strain properties for the local temperatures at the Gaussian integration points.

Output from the program included the effective, normal, and shear stresses, the equivalent total and plastic strains, the normal and shear total and plastic

strains, and the nodal displacements. Stress and strain output were given for the Gaussian integration points. To prevent excessive generation of computer printout, the output was restricted to high-strain regions of the model and some other locations required for comparison with the results of reference 10. Contour plots of effective stress, longitudinal stress and total strain, equivalent plastic strain, and temperature were obtained at the time increments of maximum and minimum total strain in the cycle.

Approximately 17 hours of execution time per cycle on a Univac 1100/42 computer was required to perform the elastic-plastic analyses. If some of the thermal cycle increments were condensed, it should be possible to run a cyclic elastic analysis with about an order of magnitude less computer time than was necessary for a two-cycle elastic-plastic analysis.

### Finite-Element Model

The finite-element model is illustrated in figure 4. Because of symmetry only one-fourth of the wedge specimen needed to be modeled; this model was the volume enclosed by the surface and intersecting midchord and midspan planes of symmetry. The element used was a 20-node, isoparametric, three-dimensional block with 8 corner nodes and 12 edge midpoint nodes. This element had 27 Gaussian integration points. The model consisted of 36 of these elements with a total of 315 nodes and 778 unsuppressed degrees of freedom.

All nodes initially on the midspan and midchord faces of the model were constrained to lie on the midspan and midchord planes, respectively. In addition, one node at the leading edge was constrained chordwise (leading to trailing edge) in order to prevent rigid-body motion in that direction.

## Results and Discussion

The results of the MARC elastic and elastic-plastic analyses of thermally cycled double-edge wedge specimens of IN 100, Mar-M 200, NASA TAZ-8A, and René 80 alloys are discussed herein. Elastic results from MARC are compared with results of ISO3DQ and NASTRAN analyses taken from reference 10 for the same alloys and cycling conditions. MARC elastic and elastic-plastic stress-strain-temperature histories are then compared for each case at the critical location (the location where the maximum total strain range occurred). Finally MARC elastic-plastic results for the four alloys are evaluated, and predicted crack locations are compared with experimental results.

### Comparison of MARC, ISO3DQ, and NASTRAN Elastic Analyses

Elastic analyses using MARC were performed by

treating each of the 34 time increments into which the thermal cycle was subdivided as separate steady-state conditions. Figures 5 and 6 show a comparison of MARC results with the results from similar elastic analyses using ISO3DQ and NASTRAN that are presented in reference 10. The finite-element models in the order from finest to coarsest were the NASTRAN model with 354 solid 8-node elements, the ISO3DQ model with 64 solid 12-node elements, and the MARC model with 36 solid 20-node elements. The MARC results shown in figures 5 and 6 apply to locations close to the span positions indicated in the figures but not exactly at those span positions because of differences in the finite-element models and in program output modes.

In figure 5 stress solutions from NASTRAN, ISO3DQ, and MARC are compared for IN 100 after 15 seconds into the heating part of the cycle. Longitudinal stresses are shown along the midchord at one-quarter span, which was approximately the critical span location for this case. The results from the three programs are in close agreement. As expected, the relatively hot leading and trailing edges were in compression.

In figure 6 longitudinal stresses calculated from ISO3DQ and MARC at leading-edge critical locations are shown as a function of cycle time for each alloy. The highest compressive stresses were reached during the first 30 seconds of heating and the highest tensile stresses during the first 15 seconds of cooling. Good agreement is shown in figure 6 between the ISO3DQ and MARC elastic analyses.

### Comparison of MARC Elastic and Elastic-Plastic Analyses

The results of the MARC elastic and elastic-plastic analyses are presented in figure 7 for each of the four alloys in terms of the effective stress-equivalent total strain response at the critical location. To construct the stress-strain hysteresis loops from the effective stresses and equivalent strains, which are always calculated as positive values, signs were assigned based on those of the principal stresses or strains with the greatest magnitude at the time increment under consideration. Critical locations shown in figure 7 were only approximate since the total strains were relatively constant over large regions of both leading and trailing edges. The apparent contradiction between the critical locations in figures 7(b), (c), and (d), which were based on MARC elastic-plastic analyses, and those in figure 6, based on ISO3DQ analyses from reference 10, was due to the ISO3DQ analyses excluding from consideration any location not at the leading edge. Elapsed times during the heating and cooling phases of the thermal cycle are indicated in figure 7.

Elastic-plastic analyses were performed for two cycles for IN 100, Mar-M 200, NASA TAZ-8A and three cycles

for René 80. The stability of the second cycle was shown by the cooling part of the stress-strain hysteresis loop essentially coinciding with that of the first cycle for the IN 100 (fig. 7(a)), Mar-M 200 (fig. 7(b)), and NASA TAZ-8A (fig. 7(c)) alloys. For the René 80 the strain ratchetting of the stress-strain hysteresis loops shown in figure 7(d) continued for a third cycle, at which time the elastic-plastic analysis was terminated; this cycle is not shown because it would have unnecessarily complicated the figure.

The results show that the wedge edges went into compression during the heating part of the cycle and reached minimum strains after 9 to 30 seconds immersion in the heating bed. As the metal temperatures approached equilibrium, the strains increased and became tensile during the cooling part of the cycle. Maximum strains occurred after 3 to 15 seconds immersion in the cooling bed. The elastic-plastic analyses exhibited compressive plastic strains at the critical locations during heating and plastic strain reversal during cooling for all the alloys. These plastic strains caused the hysteresis loops to shift under cycling as shown in figure 7, with René 80 experiencing the greatest and NASA TAZ-8A the least shifting.

The strain ranges and mean stress levels from the hysteresis loops of figure 7 are summarized in figure 8 in bar graph form for convenience of comparison. As shown in figure 8(a) the equivalent total strain ranges at the critical locations computed from elastic analyses were within 3 percent of those computed from the more costly elastic-plastic analyses. However, mean effective stresses derived from the two types of analysis were significantly different, as shown in figure 8(b). Elastic analyses calculated compressive mean stresses at the critical locations for all the alloys. For IN 100 and NASA TAZ-8A the elastic-plastic analyses showed tensile mean effective stresses at the critical locations after two cycles. René 80, which exhibited the greatest plastic flow, showed an increased mean stress in the compressive direction.

### Comparison of Elastic-Plastic Results for Alloys

Temperature-stress-strain distributions along the specimen midchord plane are displayed in figure 9 at the time of minimum strain and in figure 10 at the time of maximum strain for the four alloys. The contour plots of temperature, effective stress, longitudinal stress and total strain, and equivalent plastic strain were obtained from the elastic-plastic analyses during the second thermal cycle.

Temperature distributions shown in figure 9 and 10 are approximately symmetrical about a longitudinal axis through the center of the model. During the heating phase of the cycle, temperatures were somewhat higher at the leading edge for IN 100 and at the trailing edge for

NASA TAZ-8A and René 80. The trailing edges were slightly hotter during the cooling phase of the cycle for all the alloys.

Effective stress (figs. 9(b) and 10(b)) and longitudinal stress (figs. 9(c) and 10(c)) distributions were also approximately symmetrical about a central longitudinal axis, especially in the upper half of the model. An exception was NASA TAZ-8A, which exhibited markedly higher stresses at the trailing edge than at the leading edge. The longitudinal total strain distributions in figures 9(d) and 10(d), which include thermal deformation components, also show little change along the wedge edges in the upper half of the model.

The relative uniformity of the temperatures, stresses, and longitudinal strains over large regions of the leading and trailing edges in figures 9 and 10 indicates that failure could be expected almost anywhere in these regions because of variations in temperatures and material properties. The predicted critical locations for crack initiation illustrated in figure 7 were based on the location in the model where the maximum equivalent total strain range was computed for the second thermal cycle. These critical locations occurred at approximately a quarter of the specimen span—at the leading edge for IN 100 and at the trailing edge for Mar-M 200, NASA TAZ-8A, and René 80. Wedge specimen cyclic test data reported in references 11 and 12 demonstrate that cracks appeared at approximately all the predicted critical locations, although initial cracking tended to occur at the leading edge. The ability to predict the crack initiation location was not substantiated because of the uniform conditions over much of the wedge edges. Therefore there was no specific critical crack initiation location. The highest equivalent plastic strains occurred along the leading edge for IN 100 and Mar-M 200 and along the trailing edge for NASA TAZ-8A and René 80, as shown by the contour plots of figures 9(e) and 10(e). René 80, which had the lowest yield strength of the four alloys, had the highest equivalent plastic strains in figures 9(e) and 10(e) and exhibited the greatest amount of stress reversal in figure 7.

The primary results of this study from the standpoint of evaluation of life prediction methods were the equivalent total strain ranges and effective mean stresses computed from the elastic-plastic analyses. These results demonstrate large variations in strain range and mean stress for the various alloys under the same thermal cycling conditions. As shown in figure 7 the variations in the maximum total strains were much greater than the variations in the minimum total strains. It is noteworthy that the greatest temperature gradients between the wedge edges and center on cooldown, as shown in figures 3 and 10(a), were (in descending order) for René 80, NASA TAZ-8A, Mar-M 200, and IN 100; this ranking also coincides with the ranking of the four alloys in terms of equivalent total strain range in figure 8. Apparently the dominant factor in determining the relative strain



ranges at the critical locations for this class of materials was the rate of cooldown of the wedge edges in the fluidized-bed tests.

The principal potential sources of error in the elastic-plastic analyses lie in inaccuracies in the input data, particularly in the material properties. NASA Lewis is currently engaged in a major program to improve the quality of the input data required for cyclic nonlinear analyses. The analytical results from this study will be used for the further development of life prediction methods, such as evaluation of the applicability of various life prediction methods to thermally cycled multiaxial structures. The results of the elastic-plastic analyses will also be used to develop experimental methods for low-cycle fatigue life prediction by reproducing the stress-strain-temperature histories at the critical locations in laboratory tests of simple specimens and comparing the cycles to failure of these specimens with those of the wedge specimens.

## Summary of Results

Three-dimensional, finite-element analyses were performed with the MARC nonlinear, structural computer program for double-edge wedge specimens of four nickel-base alloys (IN 100, Mar-M 200, NASA TAZ-8A, and René 80) subjected to thermal cycling in fluidized beds. The major results of this study were as follows:

1. Maximum equivalent total strain ranges calculated from elastic analyses agreed within 3 percent of those calculated from elastic-plastic analyses.

2. Mean effective stresses calculated from elastic and elastic-plastic analyses at the critical locations were significantly different. Elastic analyses always resulted in compressive mean stresses. Elastic-plastic analyses showed tensile mean stresses in two cases. However, in the highest plastic strain case the mean stress became more compressive.

3. All the alloys exhibited plastic strain reversal at the critical locations. This caused a shifting of the stress-strain hysteresis loops from the elastic-plastic analyses.

4. The ability to predict the crack initiation location was not substantiated because of the uniformity of the temperatures, stresses, and total strains over large regions of the leading and trailing edges.

5. The dominant factor in determining the relative total strain ranges at the critical locations for this class of materials was the maximum total strain caused by the rate of cooldown of the wedge edges. The minimum total strain during the heating part of the cycle showed relatively small variation among the four alloys.

6. Comparisons of MARC elastic-analysis results with previously reported analytical results from the NASTRAN and ISO3DQ computer programs were in

good agreement even though the finite-element models were substantially different.

Lewis Research Center

National Aeronautics and Space Administration

Cleveland, Ohio, December 23, 1980.

## References

1. Hirschberg, Marvin H.; and Halford, Gary R.: Use of Strainrange Partitioning to Predict High-Temperature Low-Cycle Fatigue Life. NASA TN D-8072, 1976.
2. Saltsman, James F.; and Halford, Gary R.: Application of Strainrange Partitioning to the Prediction of Creep-Fatigue Lives of AISI Types 304 and 316 Stainless Steel. *J. Pressure Vessel Technol.*, vol. 99, no. 2, May 1977, pp. 264-271.
3. Hirschberg, Marvin H.; and Halford, Gary R.: Strainrange Partitioning—A Tool for Characterizing High-Temperature Low-Cycle Fatigue. NASA TM X-71691, 1975.
4. Halford, Gary R.; Saltsman, James F.; and Hirschberg, Marvin H.: Ductility Normalized-Strainrange Partitioning Life Relations for Creep-Fatigue Life Predictions. NASA TM-73737, 1977.
5. Manson, S. S.; Halford, Gary R.; and Hirschberg, Marvin H.: Creep Fatigue Analysis by Strain-Range Partitioning. Design for Elevated Temperature Environment, S. G. Zamrik, ed., American Society of Mechanical Engineers, 1971, pp. 12-24.
6. Spera, David A.; and Grisaffe, Salvatore J.: Life Prediction of Turbine Components. On-Going Studies at the NASA Lewis Research Center. NASA TM X-2664, 1973.
7. Bizon, P. T.; and Spera, David A.: Comparative Thermal Fatigue Resistances of Twenty-Six Nickel and Cobalt-Base Alloys. NASA TN D-8071, 1975.
8. The NASTRAN User's Manual: Level 16.0 Supplement. NASA SP-222(03), 1976.
9. User's Manual—Programs MESH3, ISO3DQ, and PROUT3 Turbine Engine Components Stress Simulation Program. (REPT. 74-2108602)-1A, AiResearch Mfg. Co., Mar. 1977.
10. Drake, S. K.; et al: Three-Dimensional Finite-Element Elastic Analysis of a Thermally Cycled Double-Edge Wedge Geometry Specimen. NASA TM-80980, 1980. (AFWAL-TR-80-2013, AD-A083245.)
11. Howes, M. A. H.: Thermal Fatigue Data on 15 Nickel- and Cobalt-Base Alloys. (IITRI-B6078-38, IIT Research Institute; NASA Contract NAS3-9411.) NASA CR-72738, 1970.
12. Howes, M. A. H.: Additional Thermal Fatigue Data on Nickel- and Cobalt-Base Superalloys. (IITRI-B6107-34, IIT Research Institute; NASA Contract NAS3-14311.) NASA CR-121211, 1973.
13. MARC General Purpose Finite Element Analysis Program. User Manual, Vols. A and B. MARC Analysis Research Corporation, 1979.
14. Kaufman, Albert; and Gaugler, Raymond E.: Cyclic Structural Analyses of Air-Cooled Gas Turbine Blades and Vanes. SAE Paper 760918, 1976. (Also NASA TM X-73494, 1976.)
15. Kaufman, Albert; and Gaugler, Raymond E.: Nonlinear, Three-Dimensional Finite-Element Analysis of Air-Cooled Gas Turbine Blades. NASA TP-1669, 1980.
16. Kaufman, Albert: Comparison of Elastic and Elastic-Plastic Structural Analyses for Cooled Turbine Blade Airfoils. NASA TP-1679, 1980.
17. Fritz, L. J.; and Koster, W. P.: Tensile and Creep Rupture Properties of (16) Uncoated and (2) Coated Engineering Alloys at Elevated Temperatures. (REPT-931-21300, Metcut Research Associates, Inc.; NASA Contract NAS3-18911.) NASA CR-135138, 1977.

TABLE I. - ALLOYS AND CONDITIONS ANALYZED

Alloys	Fluidized-bed cycling conditions for all alloys
IN 100, Mar-M 200, NASA TAZ-8A, and René 80	Heating bed temperature, 1088° C Cooling bed temperature, 316° C Immersion time in each bed, 180 seconds

TABLE II. - ALLOY PHYSICAL PROPERTIES

Temperature, °C	IN 100		Mar-M 200	
	Modulus of elasticity, MN/m <sup>2</sup>	Mean coefficient of thermal expansion, <sup>a</sup> m/m °C	Modulus of elasticity, MN/m <sup>2</sup>	Mean coefficient of thermal expansion, <sup>a</sup> m/m °C
260	203×10 <sup>3</sup>	13.0×10 <sup>-6</sup>	210×10 <sup>3</sup>	12.2×10 <sup>-6</sup>
316	199	13.1	207	12.4
371	197	13.3	205	12.6
427	194	13.5	201	12.8
482	191	13.7	199	13.0
538	187	13.9	194	13.1
593	184	14.0	191	13.3
649	180	14.4	188	13.5
704	177	14.6	182	13.7
760	173	14.9	178	14.0
816	168	15.4	173	14.2
871	162	15.8	168	14.8
927	157	16.4	163	15.1
962	151	16.7	158	15.8
1038	145	17.5	152	16.7
1093	139	18.2	147	17.6
Poisson's ratio	0.2981		0.3039	
	NASA TAZ-8A		René 80	
260	202×10 <sup>3</sup>	12.1×10 <sup>-6</sup>	188×10 <sup>3</sup>	12.4×10 <sup>-6</sup>
316	201	12.1	186	12.6
371	199	12.2	184	12.8
427	198	12.4	181	13.0
482	197	12.6	179	13.1
538	194	12.8	174	13.3
593	192	12.8	172	13.5
649	190	13.0	168	13.7
704	187	13.1	164	14.0
760	183	13.3	159	14.4
816	178	13.5	154	14.8
871	168	13.9	147	15.1
927	146	14.2	139	15.7
982	139	14.6	126	16.2
1038	133	14.9	122	16.7
1097	128	15.3	114	17.5
Poisson's ratio	0.3166		0.3183	

<sup>a</sup>From room temperature to indicated temperature.

TABLE III. - ALLOY MECHANICAL PROPERTIES (MONOTONIC)

Alloy	Temperature, °C	Ultimate strength, MN/m <sup>2</sup>	0.02-Percent yield strength, MN/m <sup>2</sup>	0.2-Percent yield strength, MN/m <sup>2</sup>	Reduction in area, percent
IN 100 (Jocoat)	21	986	614	765	14
	850	765	607	731	8
	925	565	345	462	12
	1000	386	200	296	20
Mar-M 200	21	1041	758	889	11
	871	800	558	738	4
	927	655	434	558	4
	982	510	303	393	5
NASA TAZ-8A	21	993	689	821	6
	850	848	538	745	6
	925	648	338	517	7
	1000	469	234	365	11
René 80	21	993	689	820	6
	850	683	421	538	29
	925	510	276	359	33
	1000	331	172	228	33

TABLE IV. - TEMPERATURE VARIATION ALONG SPAN

$[T_{x,z} = T_{x,ms} (Az^2 + Bz + C)]$ , where  $T_{x,z}$  is temperature at any  $x, z$  coordinate (fig. 4),  $T_{x,ms}$  is temperature at  $x$  coordinate at midspan, and  $z$  is span coordinate.]

Time increment, sec	Heating bed			Cooling bed		
	A	B	C	A	B	C
	Temperature, °C					
0	-0.00870	0.0517	0.9205	-0.00666	0.03957	0.9427
3	.04401	-.2614	1.3891	-.01775	.1055	.8447
6	.03739	-.2221	1.3290	-.02384	.1416	.7911
9	.03688	-.2191	1.3372	-.02548	.1514	.7786
12	.03806	-.2261	1.3344	-.02731	.1622	.7622
15	.03695	-.2195	1.3300	-.02889	.1716	.7480
30	.02758	-.1638	1.2504	-.03047	.1810	.7338
45	.01769	-.1051	1.1630	-.03141	.1866	.7224
60	.01432	-.08506	1.1324	-.03442	.2044	.6905
75	.01006	-.05978	1.0934	-.03265	.1939	.7093
90	.00833	-.04948	1.0791	-.02867	.1703	.7440
105	.00557	-.03311	1.0528	-.02445	.1452	.7843
120	.00627	-.03722	1.0571	-.02276	.1352	.7981
135	.00440	-.02614	1.0415	-.01876	.1142	.8323
150	.00371	-.02205	1.0357	-.01533	.09107	.8622
165	.00297	-.01762	1.0285	-.01278	.07593	.8832
180	.00262	-.01553	1.0243	-.01212	.07198	.8876

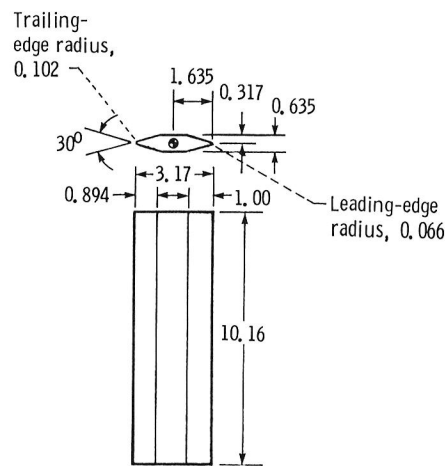


Figure 1. - Double-edge wedge. (All linear dimensions in centimeters.)

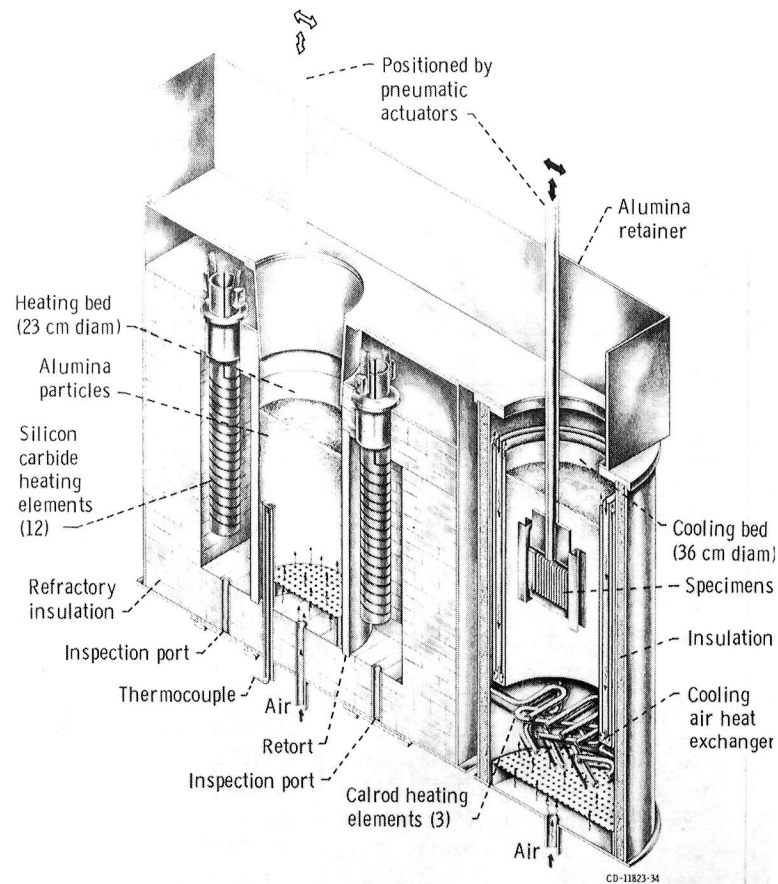


Figure 2. - Schematic of fluidized-bed test facility.

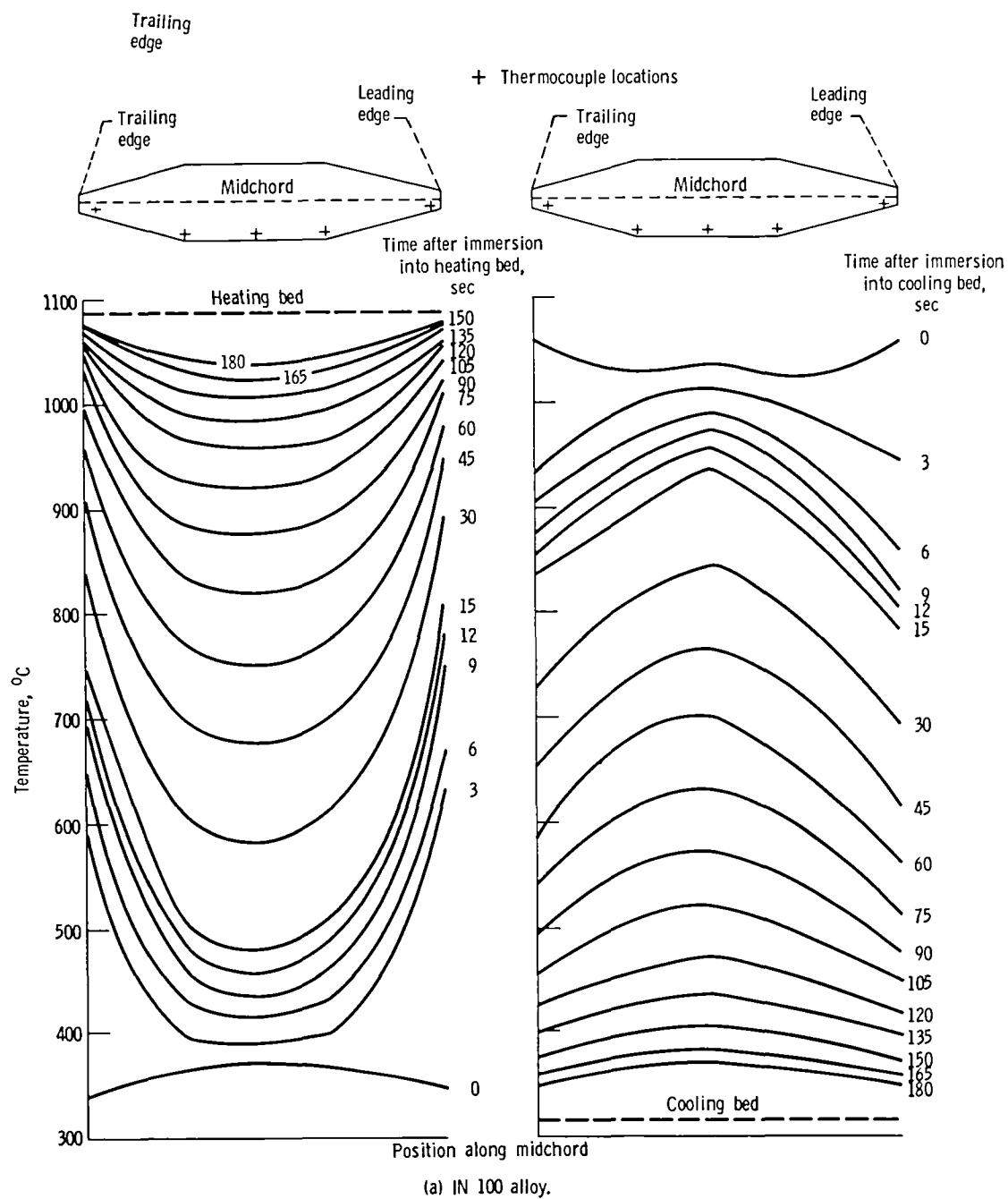
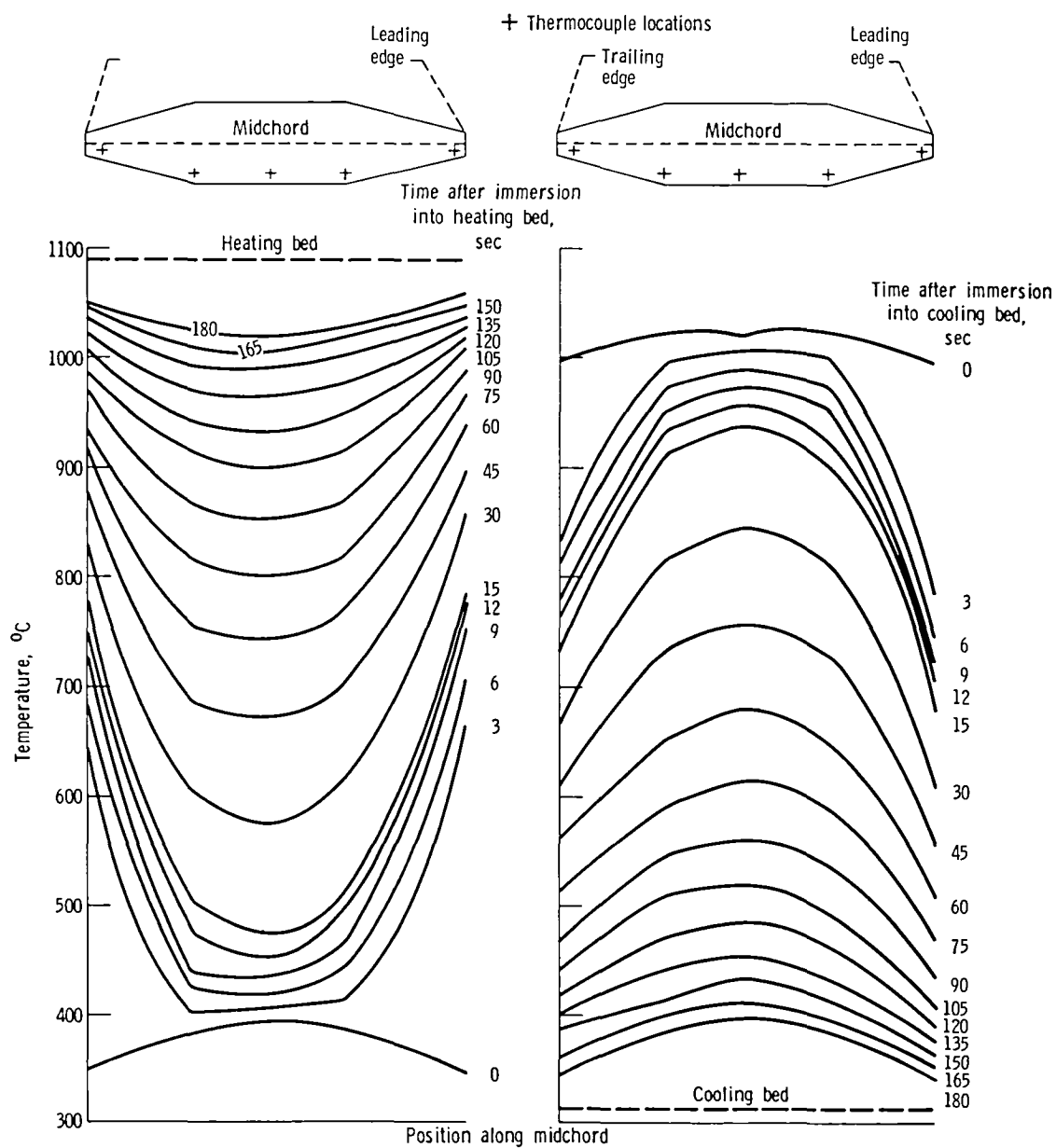


Figure 3. - Temperature of midchord at midspan at various times after immersion into fluidized beds.



(b) Mar-M 200 alloy.

Figure 3. - Continued.

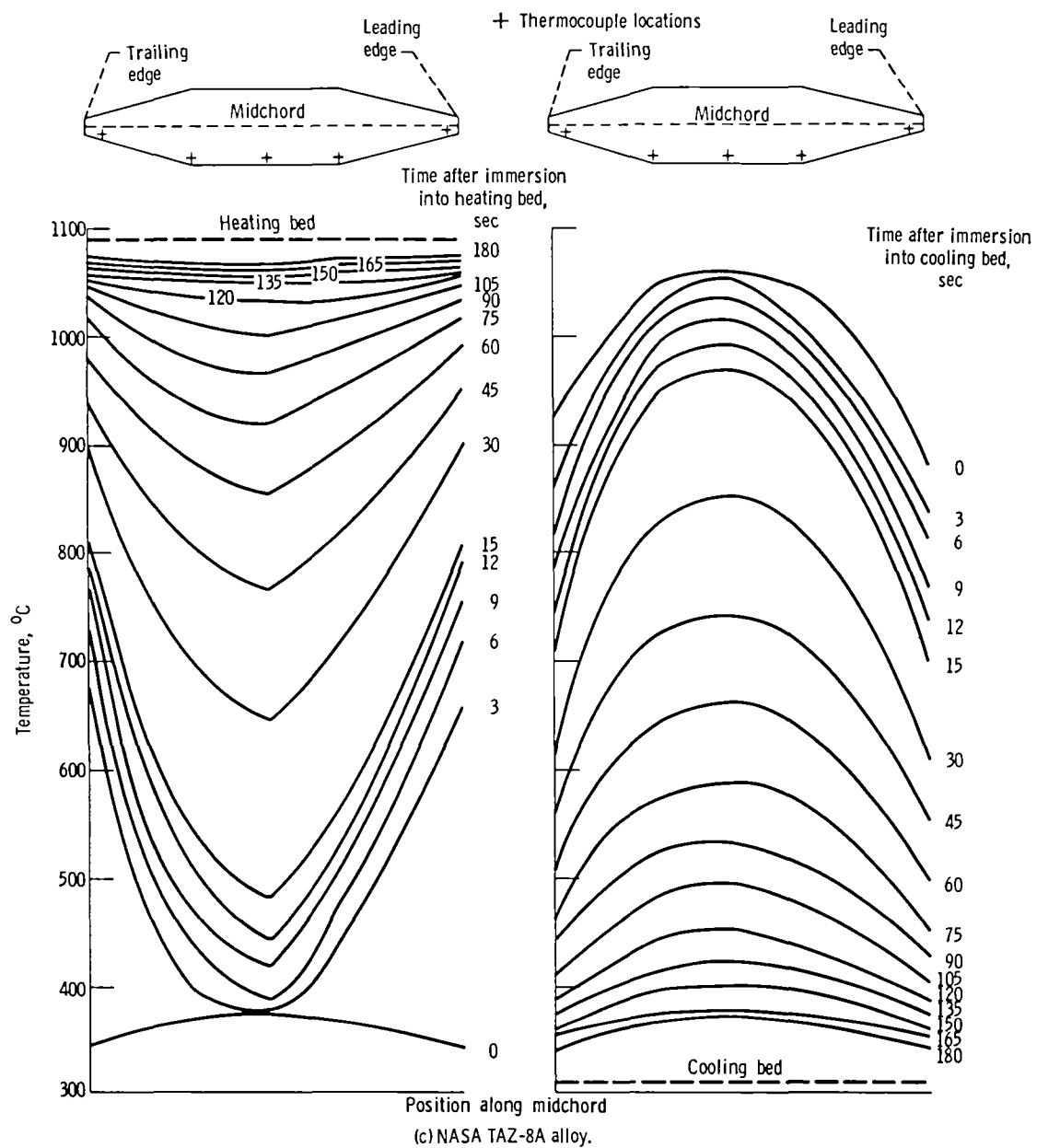
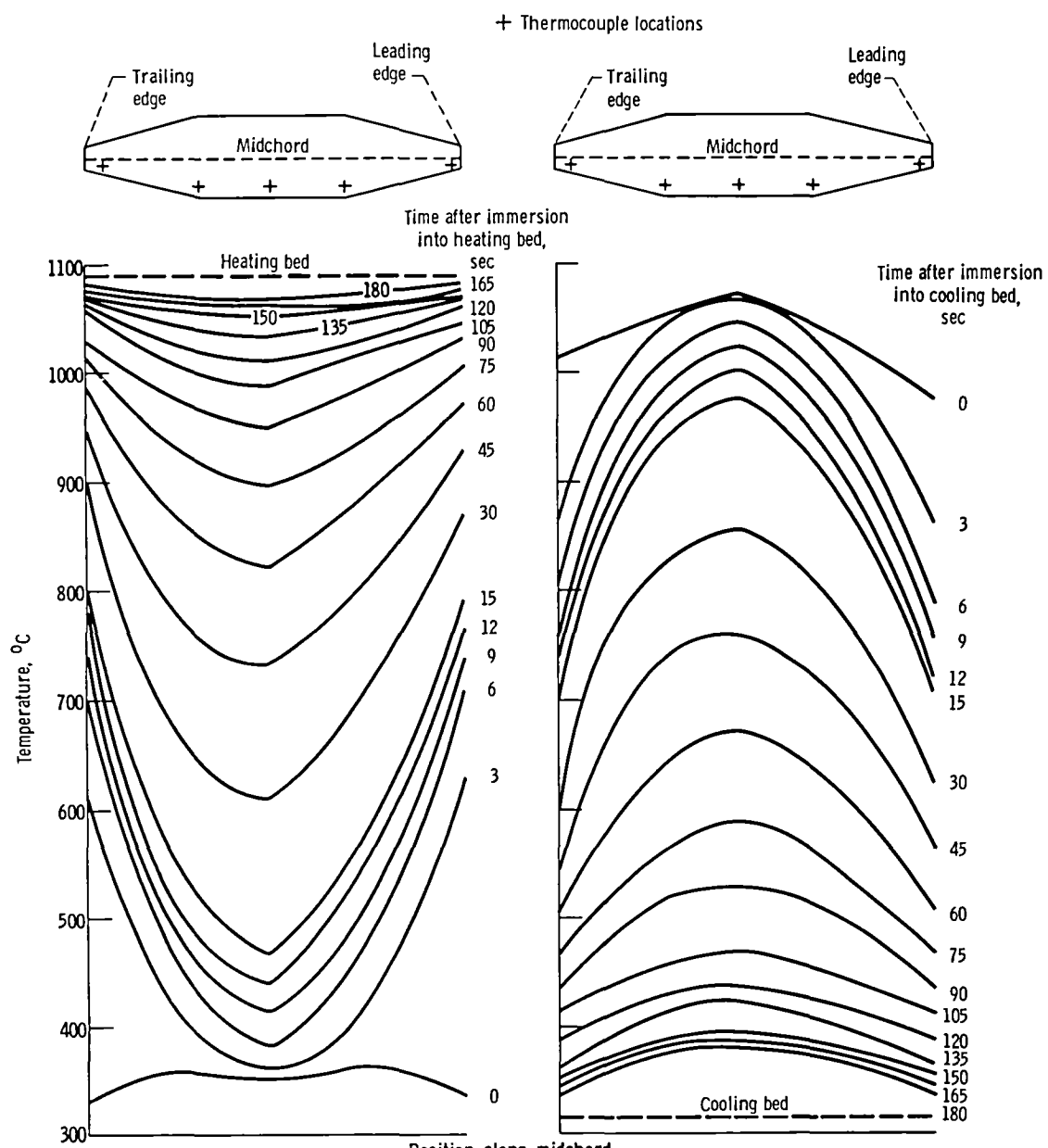


Figure 3. - Continued.





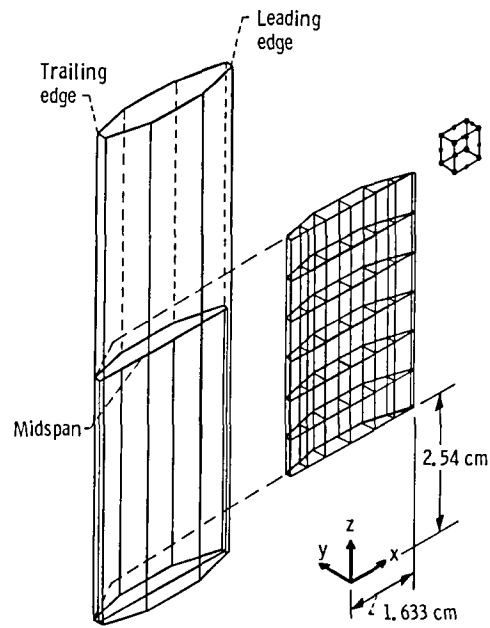


Figure 4. - Model and typical element used for MARC analysis with coordinate convention.

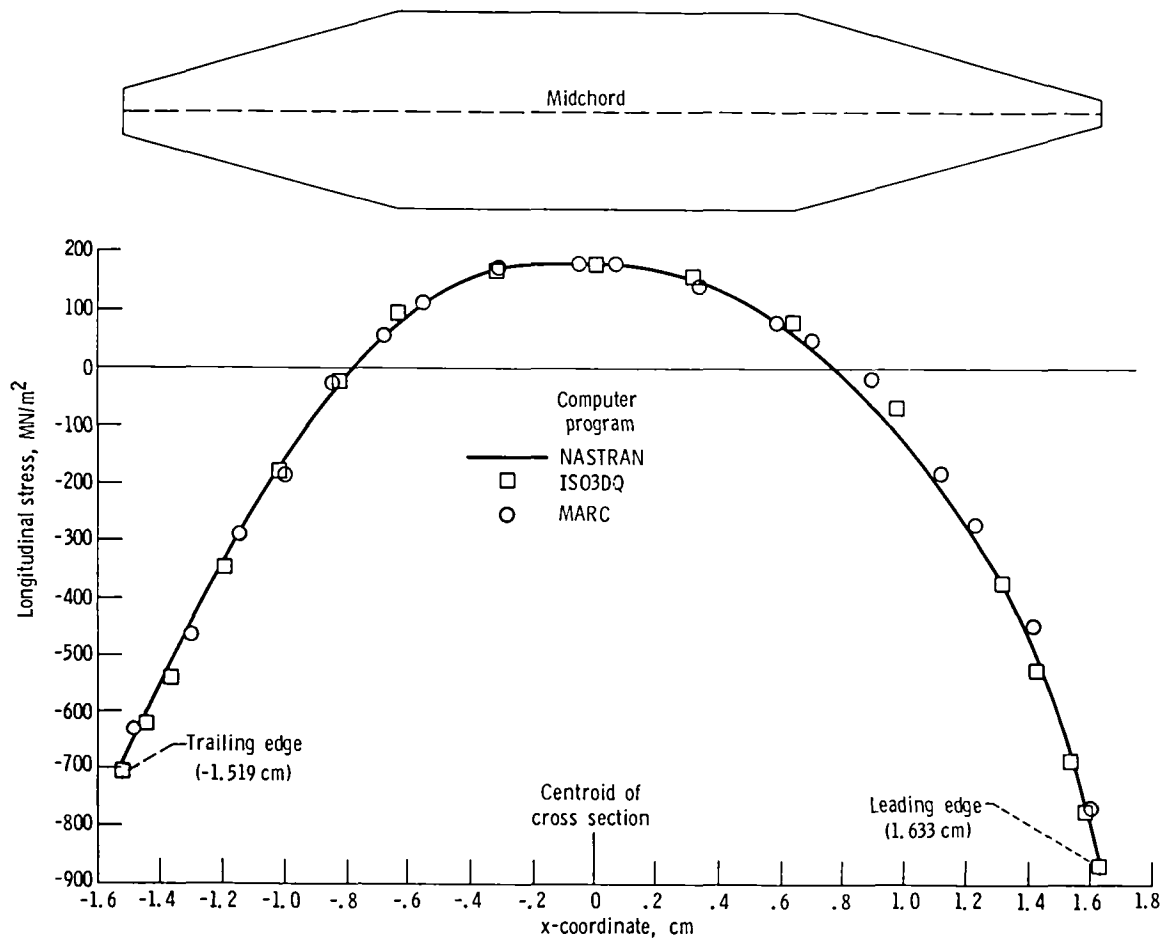


Figure 5. - Comparison of elastic results using MARC, ISO3DQ, and NASTRAN computer programs for IN 100 alloy after 15 seconds heating (along midchord at  $z = 5.08$  cm).

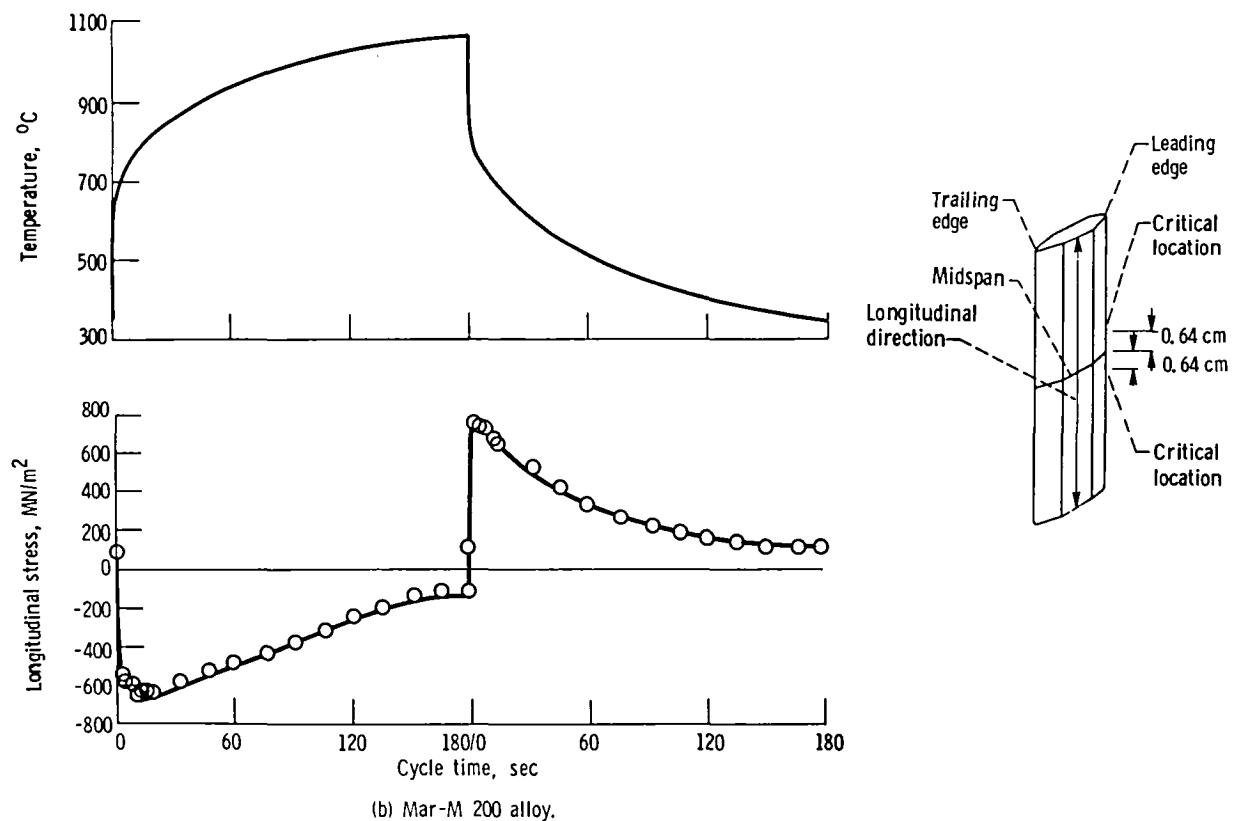
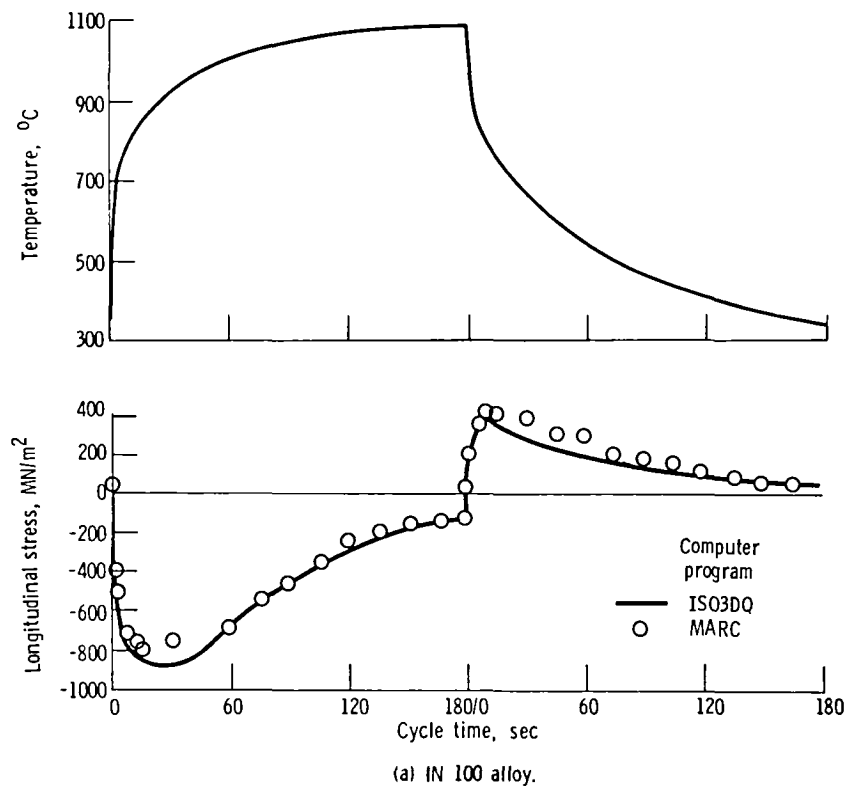
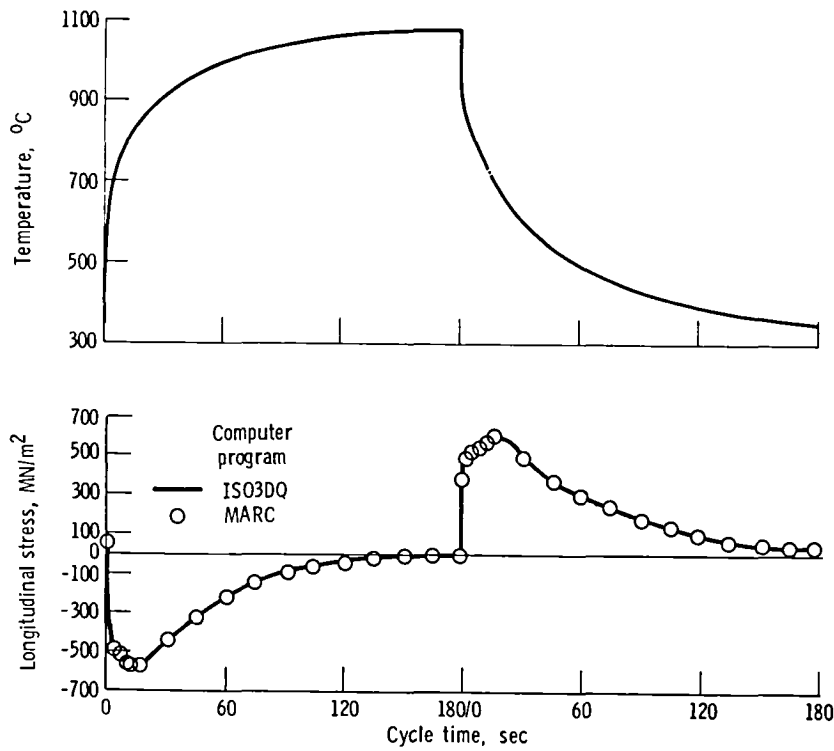
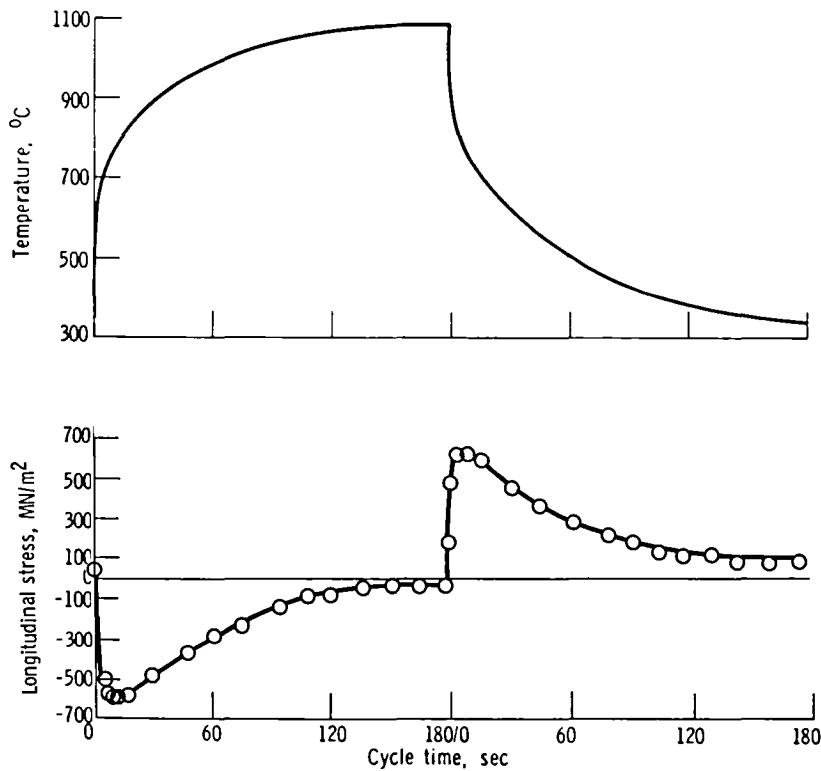
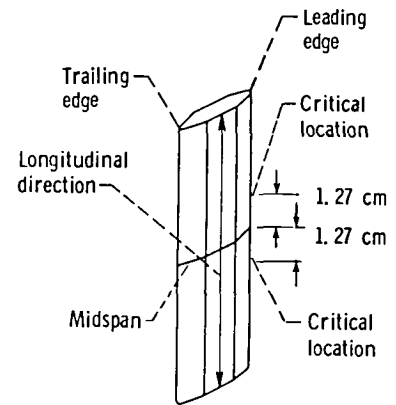


Figure 6. - Comparisons of elastic results using MARC and ISO3DQ computer programs at critical locations during a typical thermal cycle.



(c) NASA TAZ-8A alloy.



(d) René 80 alloy.

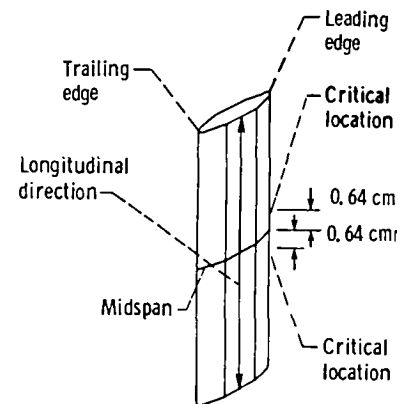


Figure 6. - Concluded.

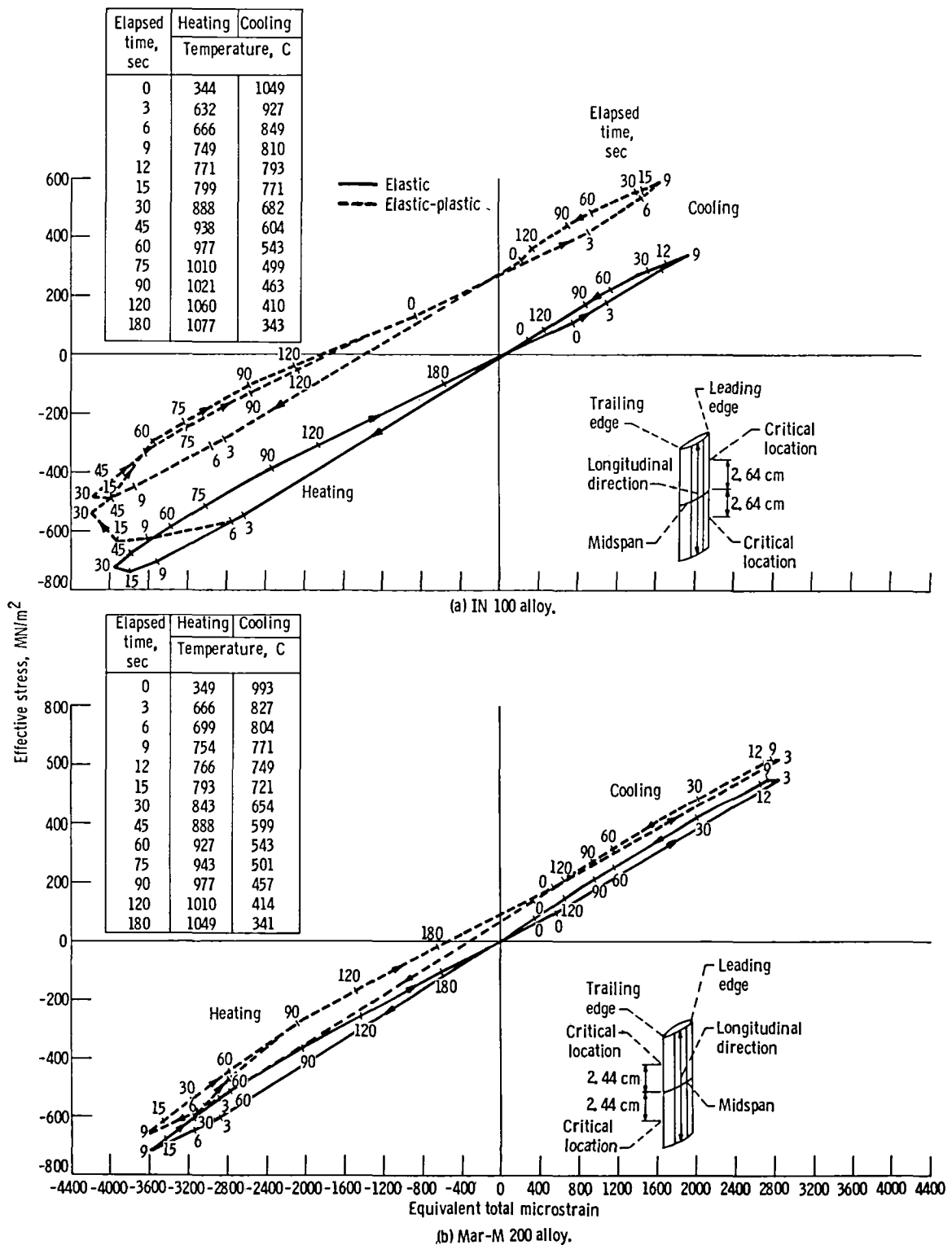
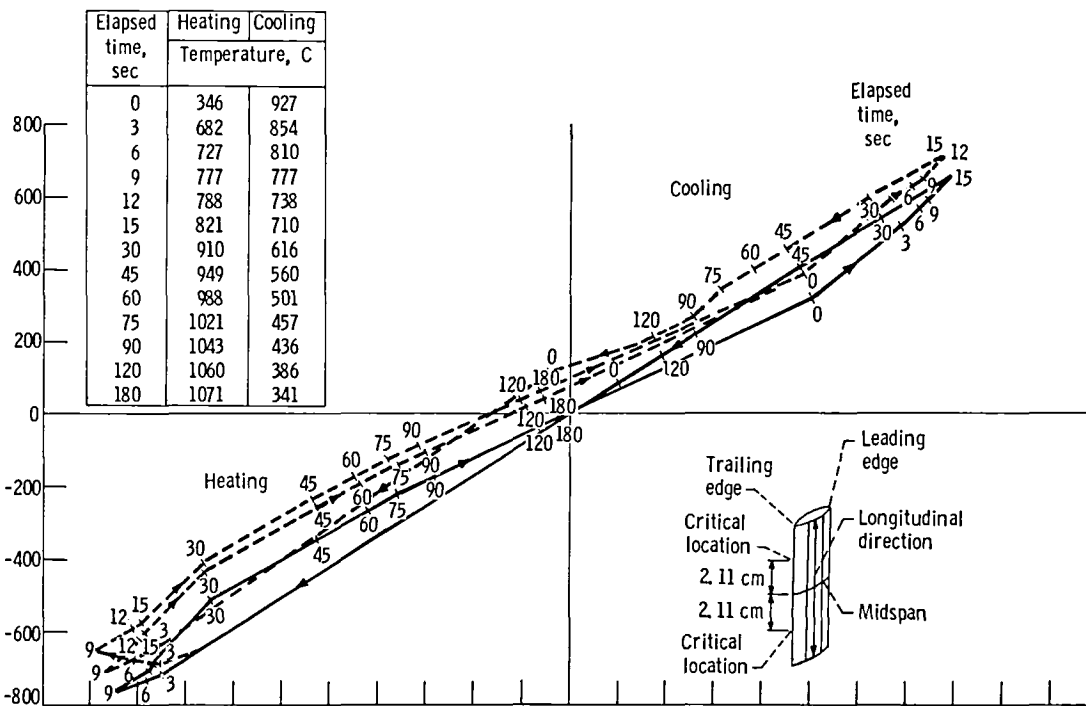
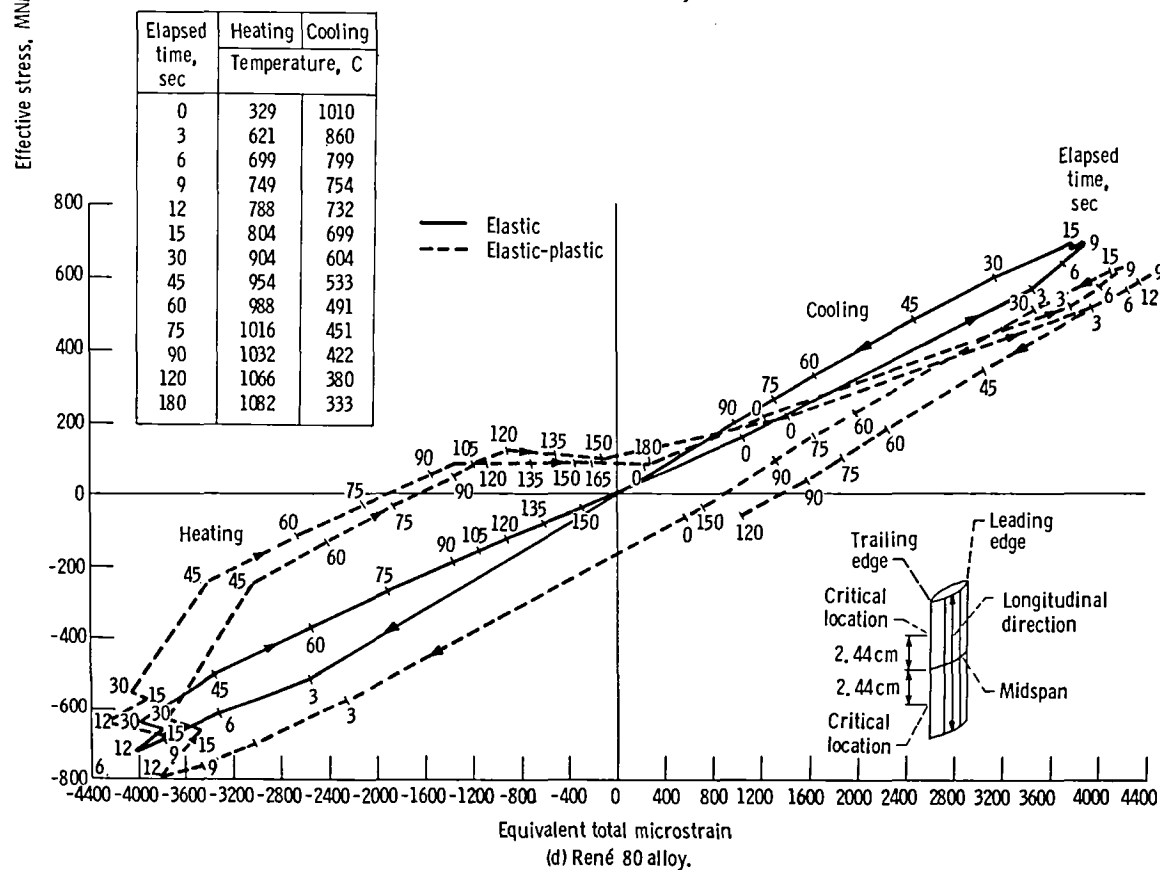


Figure 7. - Stress-strain response at critical location determined from MARC elastic and elastic-plastic analyses.



(c) NASA TAZ-8A alloy.



(d) René 80 alloy.

Figure 7. - Concluded.

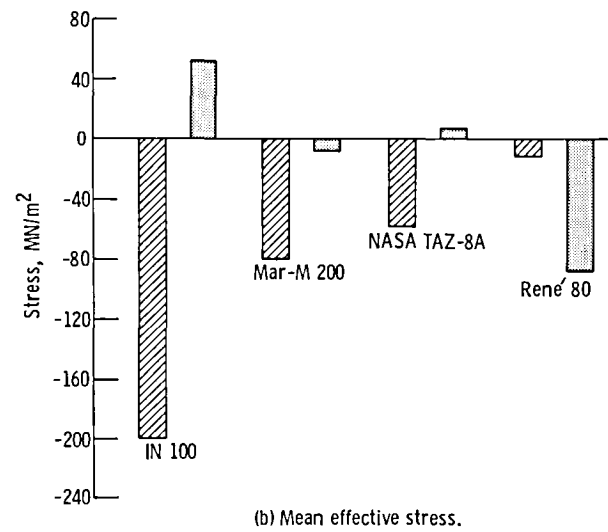
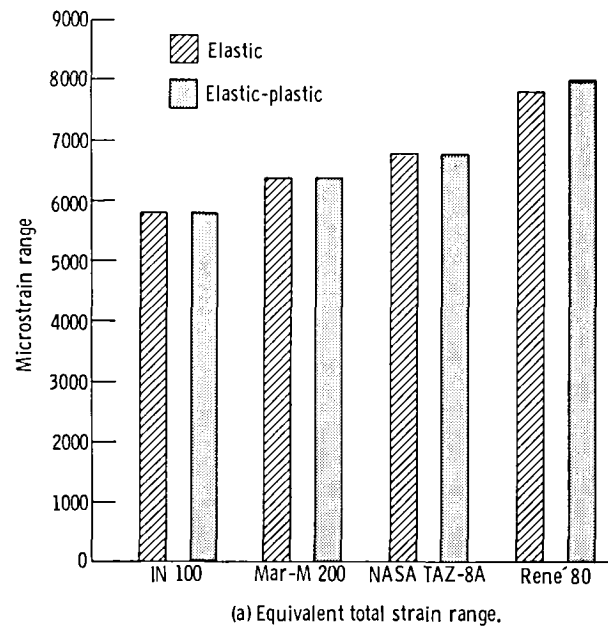
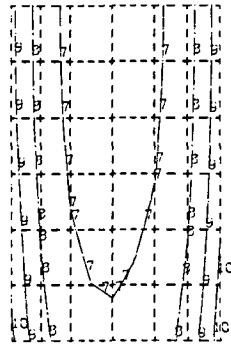


Figure 8. - Comparison of elastic and elastic-plastic (second cycle) analysis results for critical locations.

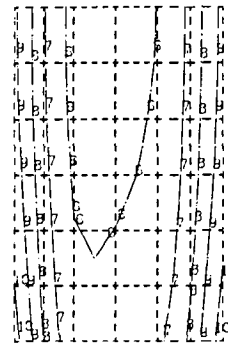
Contour	IN 100	Mar-M 200	NASA TAZ-8A	Rene' 80
	Temperature, °C			
1	33	28	26	28
2	133	120	115	121
3	233	212	204	213
4	333	304	293	306
5	433	396	382	398
6	533	488	471	491
7	633	580	560	583
8	733	672	649	676
9	833	764	738	768
10	933	856	827	860

Trailing  
edge

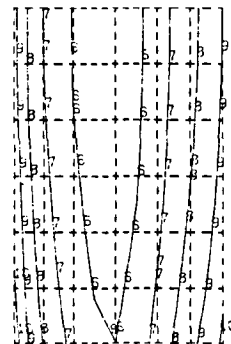
Leading edge  
Midspan



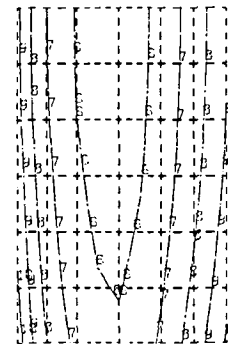
IN 100; 30 seconds heating



Mar-M 200; 9 seconds heating



NASA TAZ-8A; 9 seconds heating

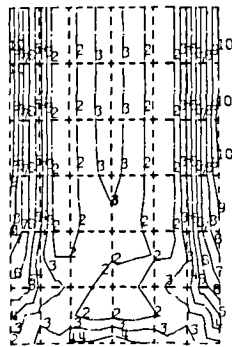


Rene' 80; 12 seconds heating

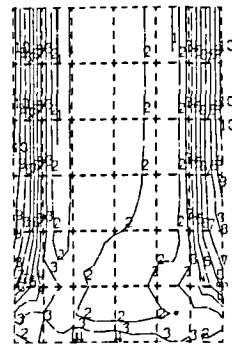
(a) Temperature.

Figure 9. - Temperature-stress-strain distributions along midchord plane at time of minimum total strain during second cycle.

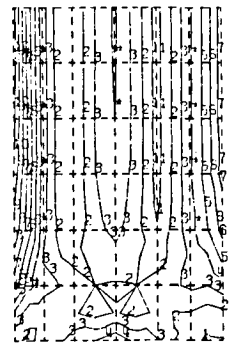
Contour	IN 100	Mar-M 200	NASA TAZ-8A	Rene' 80
	Stress, MN/m <sup>2</sup>			
1	27	36	37	39
2	83	108	111	128
3	139	179	185	217
4	195	250	259	306
5	251	322	333	395
6	307	394	407	484
7	363	465	481	573
8	419	536	555	662
9	475	607	629	751
10	531	679	703	841



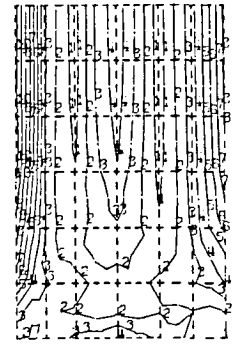
IN 100; 30 seconds heating



Mar-M 200; 9 seconds heating



NASA TAZ-8A; 9 seconds heating



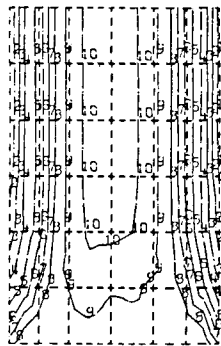
Rene' 80; 12 seconds heating

(b) Effective stress.

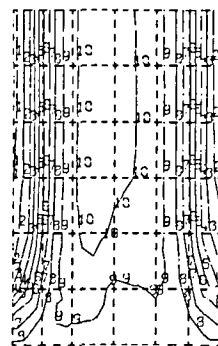
Figure 9. - Continued.



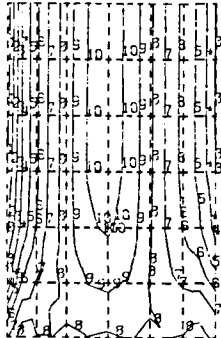
Contour	IN 100	Mar-M 200	NASA TAZ-8A	René 80
	Stress, MN/m <sup>2</sup>			
1	-556	-668	-679	-862
2	-481	-579	-589	-734
3	-407	-489	-498	-606
4	-332	-399	-407	-479
5	-258	-310	-317	-351
6	-183	-221	-226	-224
7	-109	-132	-135	-97
8	-34	-42	-45	31
9	40	48	46	158
10	115	137	137	285



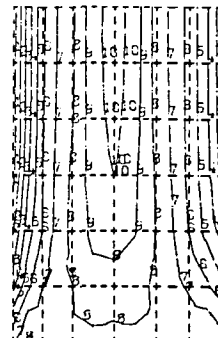
IN 100; 30 seconds heating



Mar-M 200; 9 seconds heating



NASA TAZ-8A; 9 seconds heating

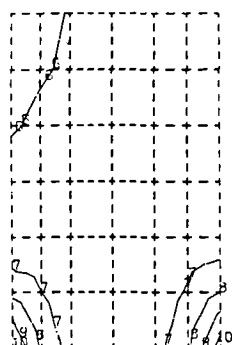


René 80; 12 seconds heating

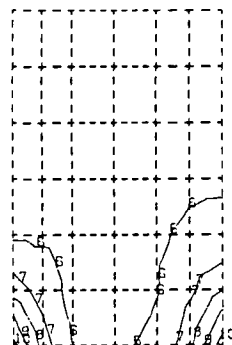
(c) Longitudinal stress.

Figure 9. - Continued.

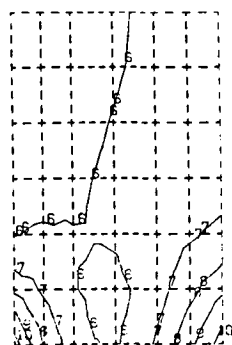
Contour	IN 100	Mar-M 200	NASA TAZ-8A	Rene' 80
	Microstrain			
1	780	620	600	660
2	2 320	1 850	1 780	1 970
3	3 870	3 080	2 990	3 280
4	5 420	4 310	4 180	4 590
5	6 970	5 540	5 370	5 900
6	8 520	6 770	6 570	7 210
7	10 100	8 000	7 760	8 530
8	11 600	9 230	8 960	9 840
9	13 200	10 500	10 200	11 100
10	14 700	11 700	11 300	12 500



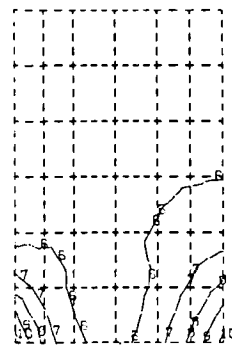
IN 100; 30 seconds heating



Mar-M 200; 9 seconds heating



NASA TAZ-8A; 9 seconds heating

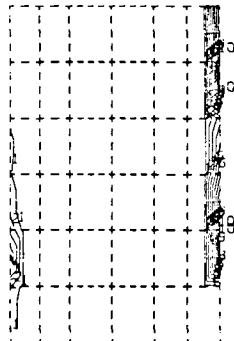


Rene 80; 12 seconds heating

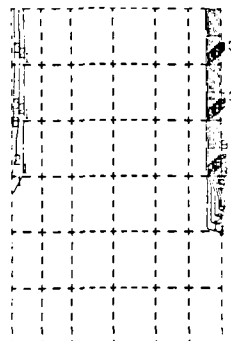
(d) Longitudinal total strain.

Figure 9. - Continued.

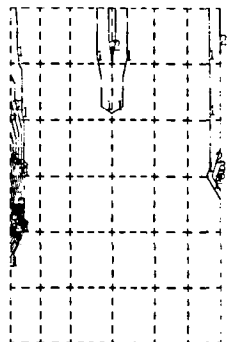
Contour	IN 100	Mar-M 200	NASA TAZ-8A	Rene' 80
	Microstrain			
1	50	50	34	14
2	270	140	100	270
3	450	230	170	530
4	630	320	240	780
5	810	410	300	1040
6	990	500	370	1300
7	1170	590	440	1550
8	1350	680	510	1810
9	1530	770	570	2070
10	1710	860	640	2320



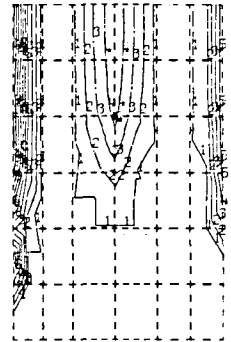
IN 100; 30 seconds heating



Mar-M 200; 9 seconds heating



NASA TAZ-8A; 9 seconds heating



Rene' 80; 12 seconds heating

(e) Equivalent plastic strain.

Figure 9. - Concluded.

Contour	IN 100	Mar-M 200	NASA TAZ-8A	Rene' 80
	Temperature, °C			
1	32	34	32	35
2	132	137	134	139
3	232	240	236	244
4	332	343	338	349
5	432	446	440	454
6	532	549	542	559
7	632	652	644	663
8	732	755	746	768
9	832	858	848	873
10	932	961	950	977

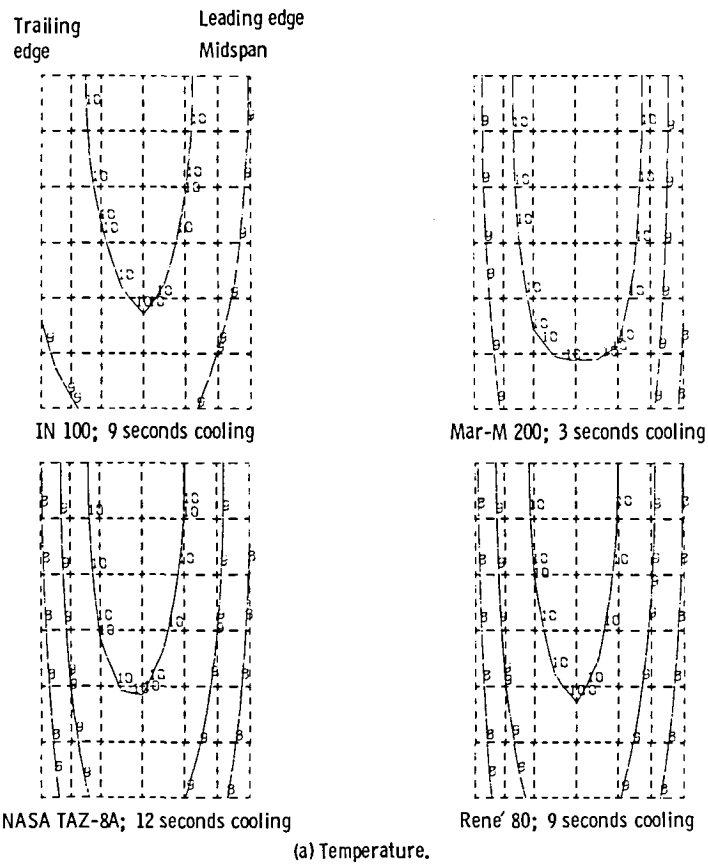
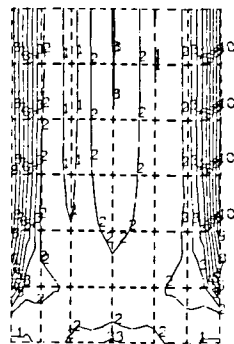
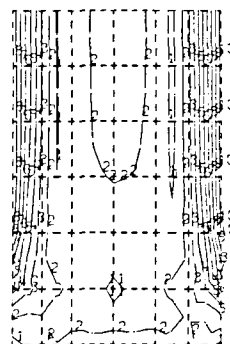


Figure 10. - Temperature-stress-strain distributions along midchord plane at time of maximum total strain during second cycle.

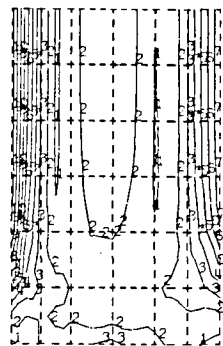
Contour	IN 100	Mar-M 200	NASA TAZ-8A	Rene' 80
	Stress, MN/m <sup>2</sup>			
1	34	42	41	34
2	103	125	122	105
3	171	209	203	176
4	238	292	285	247
5	308	376	366	318
6	376	460	447	389
7	444	543	528	459
8	513	627	609	530
9	581	710	690	601
10	649	793	772	672



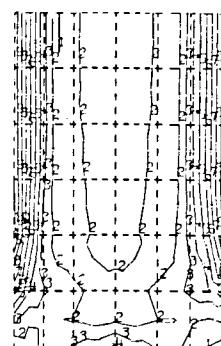
IN 100; 9 seconds cooling



Mar-M 200; 3 seconds cooling



NASA TAZ-8A; 12 seconds cooling

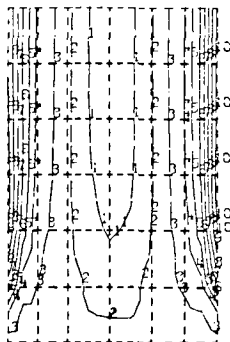


Rene' 80; 9 seconds cooling

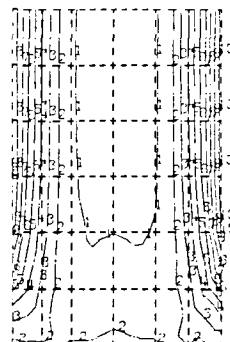
(b) Effective stress.

Figure 10. - Continued.

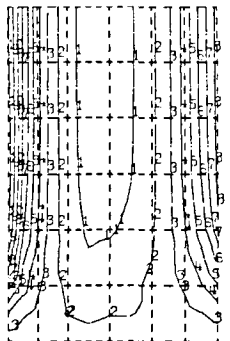
Contour	IN 100	Mar-M 200	NASA TAZ-8A	Rene' 80
	Stress, MN/m <sup>2</sup>			
1	-123	-100	-130	-127
2	-36	0	-30	-36
3	51	100	70	55
4	137	200	170	146
5	224	300	270	236
6	311	400	370	327
7	398	500	470	418
8	484	600	570	509
9	571	700	670	600
10	658	800	770	690



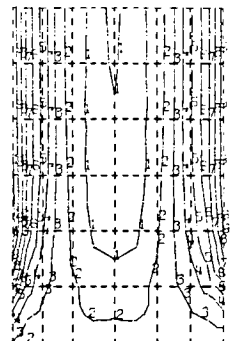
IN 100; 9 seconds cooling



Mar-M 200; 3 seconds cooling



NASA TAZ-8A; 12 seconds cooling

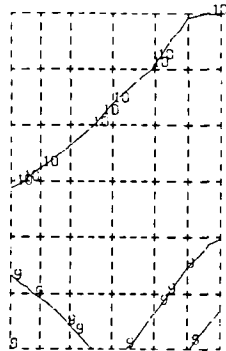


Rene' 80; 9 seconds cooling

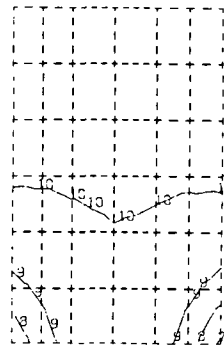
(c) Longitudinal stress.

Figure 10. - Continued.

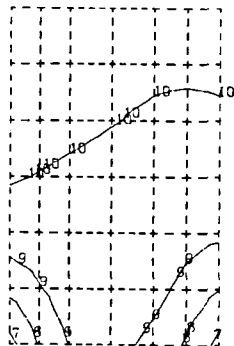
Contour	IN 100	Mar-M 200	NASA TAZ-8A	Rene' 80
	Microstrain			
1	770	770	690	770
2	2 290	2 300	2 090	2 310
3	3 820	3 830	3 480	3 850
4	5 350	5 360	4 870	5 390
5	6 880	6 900	6 270	6 930
6	8 410	8 430	7 660	8 480
7	9 940	9 960	8 050	10 000
8	11 500	11 500	10 400	11 600
9	13 000	13 000	11 800	13 100
10	14 500	14 600	13 200	14 600



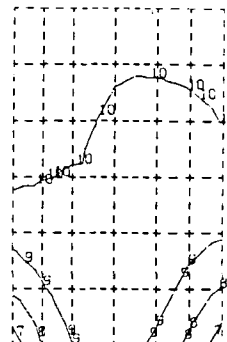
IN 100; 9 seconds cooling



Mar-M 200; 3 seconds cooling



NASA TAZ-8A; 12 seconds cooling

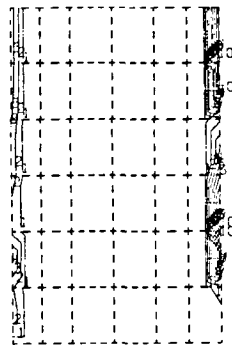


Rene' 80; 9 seconds cooling

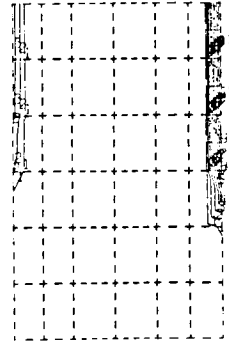
(d) Longitudinal strain.

Figure 10. - Continued.

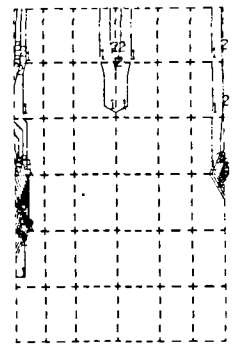
Contour	IN 100	Mar-M 200	NASA TAZ-8A	Rene' 80
	Microstrain			
1	81	60	32	70
2	250	180	100	560
3	420	320	160	1050
4	580	450	220	1540
5	750	580	290	2030
6	920	700	350	2520
7	1080	830	410	3010
8	1250	960	480	3500
9	1420	1090	540	3990
10	1580	1210	600	4480



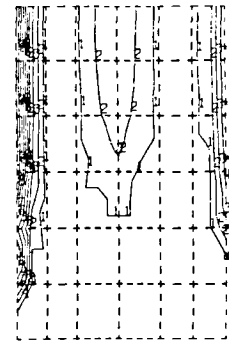
IN 100; 9 seconds cooling



Mar-M 200; 3 seconds cooling



NASA TAZ-8A; 12 seconds cooling



Rene' 80; 9 seconds cooling

(e) Equivalent plastic strain.

Figure 10. - Concluded.





1. Report No. NASA TP-1973		2. Government Accession No.		3. Recipient's Catalog No.	
4. Title and Subtitle  ELASTIC-PLASTIC FINITE-ELEMENT ANALYSES OF THERMALLY CYCLED DOUBLE-EDGE WEDGE SPECIMENS				5. Report Date March 1982	
				6. Performing Organization Code 505-33-22	
7. Author(s)  Albert Kaufman and Larry E. Hunt				8. Performing Organization Report No. E-626	
				10. Work Unit No.	
9. Performing Organization Name and Address National Aeronautics and Space Administration Lewis Research Center Cleveland, Ohio 44135				11. Contract or Grant No.	
				13. Type of Report and Period Covered Technical Paper	
12. Sponsoring Agency Name and Address National Aeronautics and Space Administration Washington, D. C. 20546				14. Sponsoring Agency Code	
15. Supplementary Notes					
16. Abstract  <p>Elastic-plastic stress-strain analyses were performed for double-edge wedge specimens subjected to thermal cycling in fluidized beds. Four cases involving different nickel-base alloys (IN 100, Mar M-200, NASA TAZ-8A, and René 80) were analyzed by using the MARC nonlinear, finite-element computer program. Elastic solutions from MARC showed good agreement with previously reported solutions obtained by using the NASTRAN and ISO3DQ computer programs. Equivalent total strain ranges at the critical locations calculated by elastic analyses agreed within 3 percent with those calculated from elastic-plastic analyses. The elastic analyses always resulted in compressive mean stresses at the critical locations. However, elastic-plastic analyses showed tensile mean stresses for two of the four alloys and an increase in the compressive mean stress for the highest plastic strain case.</p>					
17. Key Words (Suggested by Author(s)) Structures Thermal fatigue Elastic-plastic analyses			18. Distribution Statement Unclassified - unlimited STAR Category 39		
19. Security Classif. (of this report) Unclassified		20. Security Classif. (of this page) Unclassified		21. No. of Pages 30	
				22. Price* A03	

\* For sale by the National Technical Information Service, Springfield, Virginia 22161

3 1176 00511 1688

National Aeronautics and  
Space Administration

Washington, D.C.  
20546

Official Business

Penalty for Private Use, \$300

THIRD-CLASS BULK RATE

Postage and Fees Paid  
National Aeronautics and  
Space Administration  
NASA-451



**NASA**

POSTMASTER: If Undeliverable (Section 158  
Postal Manual) Do Not Return

---